CCFE-PR(16)10

C.J. Ham, R.G.J. Cramp, S. Gibson, S.A. Lazerson, I.T. Chapman and A. Kirk

Non-axisymmetric Ideal Equilibrium and Stability of ITER Plasmas with Rotating RMPs

Non-axisymmetric Ideal Equilibrium and Stability of ITER Plasmas with Rotating RMPs

C.J. Ham[1], R.G.J. Cramp[1,2], S. Gibson[3], S.A. Lazerson[4], I.T. Chapman[1,3] and A. Kirk[1]

[1]CCFE, Culham Science Centre, Abingdon, OX14 3DB, UK
[2]Department of Physics, University of Bath, Claverton Down, Bath, BA2 7AY
[3]Department of Physics, Durham University, Durham, DH1 3LE
[4]Princeton Plasma Physics Laboratory, Princeton, NJ, USA

Non-axisymmetric ideal equilibrium and stability of ITER plasmas with rotating RMPs

C J Ham[1], R G J Cramp[1,2], S Gibson[3], S A Lazerson[4], I T Chapman[1,3] and A Kirk[1]

[1]CCFE, Culham Science Centre, Abingdon, Oxon, OX14 3DB
[2]Department of Physics, University of Bath, Claverton Down, Bath, BA2 7AY
[3]Department of Physics, Durham University, Durham, DH1 3LE
[4]Princeton Plasma Physics Laboratory, Princeton, NJ, USA

E-mail: christopher.ham@ccfe.ac.uk

Abstract. The magnetic perturbations produced by the resonant magnetic perturbation (RMP) coils will be rotated in ITER so that the spiral patterns due to strike point splitting which are locked to the RMP also rotate. This is to ensure even power deposition on the divertor plates. VMEC equilibria are calculated for different phases of the RMP rotation. It is demonstrated that the off harmonics rotate in the opposite direction to the main harmonic. This is an important topic for future research to control and optimize ITER appropriately. High confinement mode (H-mode) is favourable for the economics of a potential fusion power plant and its use is planned in ITER. However, the high pressure gradient at the edge of the plasma can trigger periodic eruptions called edge localized modes (ELMs). ELMs have the potential to shorten the life of the divertor in ITER [Loarte *et al. Plasma Phys. Control. Fusion* (2003) **45** 1549] and so methods for mitigating or suppressing ELMs in ITER will be important. Non-axisymmetric RMP coils will be installed in ITER for ELM control. Sampling theory is used to show that there will be significant a $n_{coils} - n_{rmp}$ harmonic sideband. There are nine coils toroidally in ITER so $n_{coils} = 9$. This results in a significant $n = 6$ component to the $n_{rmp} = 3$ applied field and a significant $n = 5$ component to the $n_{rmp} = 4$ applied field. Although the vacuum field has similar amplitudes of these harmonics the plasma response to the various harmonics dictates the final equilibrium. Magnetic perturbations with toroidal mode number $n = 3$ and $n = 4$ are applied to a 15MA, $q_{95} \approx 3$ burning ITER plasma. We use a three-dimensional ideal magnetohydrodynamic model (VMEC) to calculate ITER equilibria with applied RMPs and to determine growth rates of infinite n ballooning modes (COBRA). The $n_{rmp} = 4$ case shows little change in ballooning mode growth rate as the RMP is rotated, however there is a change with rotation for the $n_{rmp} = 3$ case.

1. Introduction

It will be important for ITER to demonstrate operation in high confinement mode (H-mode) because this significantly improves the economics of a potential fusion power plant. However, it is well known that H-mode can suffer from periodic plasma eruptions

from the edge, called edge localized modes (ELMs). In current machines ELMs do not cause significant damage, however it is predicted in ITER that natural, type-I, ELMs will limit the lifetime of the divertor [1] and so they must be controlled. A number of potential methods for ELM control exist, such as pellet pacing and vertical kicks [2, 3], but we focus on the use of resonant magnetic perturbations (RMPs) produced by non-axisymmetric coils, near the plasma edge. Experimentally, it has been demonstrated on a number of machines that RMP coils can alter the frequency of ELMs, either increasing the frequency and thus decreasing the peak heat load (ELM mitigation) or removing the ELMs completely (ELM suppression) [5–7]. ELMs can also be useful as they are likely to remove tungsten impurities from the plasma edge which may otherwise accumulate in the plasma core and cause reduced plasma performance. This provides more motivation to understand how ELMs can be controlled.

ELMs are thought to be the nonlinear phase of the peeling-ballooning instability [8]. A significant strand of research has looked at the linear stability of the plasma to peeling-ballooing modes to understand when the plasma would be unstable to ELMs. Axisymmetric modelling of peeling-ballooning stability using ELITE [9] has been particularly successful. However, there is currently little understanding and thus predictive capability, of what occurs when RMP coils are applied to a plasma in a particular configuration. In certain circumstances axisymmetric analysis of plasmas with RMPs applied indicates that the plasma should be stable, however experimentally ELMs are still observed [10]. This indicates that the effect is due to more than the change in stability due to the loss in density often caused by the application of the RMP coils ('density pumpout'). Non-axisymmetric effects are important. There are currently no proven tools available to analyse the peeling-ballooning linear plasma stability when RMPs are applied.

The response of the plasma to the RMPs develops over several timescales. When the RMPs are switched on, a new, non-axisymmetric, equilibrium is established and this happens on an Alfvénic timescale. The new equilibrium has different stability characteristics to all of the plasma modes. This changes the turbulence and so the transport of heat and particles. The equilibrium then develops on a transport timescale. We have observed that both of these effects occur in fusion plasmas. Experimentally we see the plasma gains a non-axisymmetric midplane displacement [11,12] and also density pumpout occurs [6]. The second part of applying RMPs is that the new equilibrium has different stability characteristics to the peeling-ballooning modes, which produce the ELMs. The change in stability is due to the new profiles of pressure and current and the non-axisymmetry.

The RMP coils in ITER are made up of 27 coils arranged in three toroidal rows of nine coils in each row. It is anticipated that these coils will be used in either $n_{rmp} = 3$ or $n_{rmp} = 4$ configurations, where n_{rmp} is the toroidal mode number of the applied RMP field. The maximum current in each coil will be 90kA and each coil will have a separate power supply allowing them to be controlled independently. The optimal toroidal mode number for ELM mitigation and suppression is not known, however, toroidal mode

numbers $n = 2, 3, 4, 6$ were examined in MAST [13]. This work concluded that there was no clear optimum but that $n = 3$ and $n = 4$ were broadly preferred. A note of caution should be given over the plasma control system when RMPs are applied. Given the plasma is no longer axisymmetric the plasma will be closer to the wall in some locations than in others. If the plasma control system does not take this in to account then it may inadvertantly move the plasma too close to the wall at a given toroidal location potentially causing damage to the first wall [14].

It is expected that the currents in the RMP coils will be constantly changing so that the perturbations rotate toroidally. This is because the pattern of the plasma strike point on the divertor plates is locked to the RMP and so rotating the perturbation will spread the wear. We will describe rotation as increasing the absolute phase of the perturbation. This is not to be confused with a differential phase scan where the perturbations due to the different rows of RMP coils rotate at different rates. The RMP rotation rate is expected to slow (of the order of a few Hz) so we can consider the plasma to be in equilibrium at any point as the RMP is rotated.

In non-axisymmetric toroidal geometry there is no equivilent of the Grad-Shafranov equation. There are many approaches to modelling the response of the plasma to RMPs [15,16], linear or nonlinear, dynamic or equilibrium. The plasma equilibrium will be studied here using VMEC [17, 18], which is an energy minimization code. VMEC is a fully non-linear 3D MHD equilibrium code and it uses the steepest decent algorithm to find the minimum energy states of the plasma. The plasma energy is

$$W = \int \left(\frac{|\vec{B}|^2}{2\mu_0} + \frac{p}{\gamma - 1} \right) \mathrm{d}^3 x \tag{1}$$

where $\vec{B}$ is the magnetic field and p is the pressure, and γ is the adiabatic index. The equilibrium coil currents, pressure profile, and current density profile define the equilibrium state in free boundary VMEC (alternatively the iota profile may be specified instead of the current density) [17, 18]. VMEC assumes that the flux surfaces remain nested, so that no islands or stochastic regions can form. This may not be a fully realistic assumption as the RMP may cause small islands to be formed. However, theoretical calculations and modelling, for example with JOREK [19], indicate that diamagnetic effects and plasma rotation may cause any islands in the plasma to be much smaller than otherwise expected by a purely resistive MHD plasma [20]. Plasma rotation is not included within this model. The assumption of nested flux surfaces with non-axisymmetry implies singular currents at rational surfaces which are not physical [21]. However, VMEC serves as a useful approximation to the non-axisymmetric tokamak equilibrium. It should be noted that initial concerns raised over the validity of VMEC to to problems such as those investigated here have not been borne out by further work. Experimental tests of the plasma response [16] show that VMEC can quantitively describe the plasma response. Further work showed good agreement between a theoretical screw pinch calculation [22] and results produced by VMEC [23].

In this paper we use COBRA [24,25] to calculate the infinite n ballooning stability

of the VMEC computed ITER plasmas. It is well known that infinite n ballooning modes are correlated to kinetic ballooning modes (KBMs), which are thought to be responsible for driving turbulence that sets the maximum pressure gradient. Thus if infinite n ballooning modes become more unstable when RMPs are applied we would expect the maximum pressure gradient to be reduced. Also, infinite n ballooning stability is an approximation, in $1/n$, to finite n stability. WKB theory can be used to find the next order approximation to finite n stability [26]. Finally, COBRA is a fast code and so results can be quickly obtained.

In Section 2 we investigate the equilibria produced using $n_{rmp} = 3$ and $n_{rmp} = 4$ RMPs. In Section 3 we investigate the change caused to the plasma stability by the application of the RMPs. We further investigate if the change in stability is constant with the rotation of the RMPs. We give some discussion and conclusions in Section 4.

2. Equilibrium

2.1. Axisymmetric equilibrium

We use a 15MA burning ITER H-mode plasma as modelled by Lazerson [27] and Liu [28, 29] as our base case. In Lazerson [27] plasma pressure and current profiles arising from axisymmetric transport modelling, using CORSICA, of an ITER H-mode plasma were used along with the locations of the toroidal and poloidal field coils to produce a free boundary VMEC equilibrium. It should also be noted that the enclosed toroidal flux was optimized so that the axisymmetric equilibrium fit inside the CORSICA separatrix. The flux surfaces of the axisymmetric equilibrium are shown in figure 1. The computed safety factor profile is shown in figure 2. This matches the CORSICA safety factor profile well, as shown in [27]. Finally, the pressure profile is shown in figure 3. Notice the pedestal near to the plasma edge which is characteristic of an H-mode plasma.

2.2. Sampling and aliasing

The RMP perturbation would ideally be applied as one toroidal harmonic. However, a finite number of coils toroidally are used to produce a given perturbation. If there were a large number of coils compared to the toroidal mode number then the ideal RMP would be well represented. However, in ITER there will be nine coils toroidally in each of the three rows which means that aliasing may be a problem.

We wish to apply a single toroidal harmonic magnetic perturbation to the plasma. We do this by passing currents through the RMP coils. The ideal current in the coils would have the form [30]

$$I_{pert} = I_0 \cos(n_{rmp}(\phi - \phi_0)) \tag{2}$$

where ϕ is toroidal angle, n_{rmp} is the toroidal harmonic of the RMP applied and ϕ_0 is an arbitrary phase. However, this ideal current is sampled at each actual RMP coil location

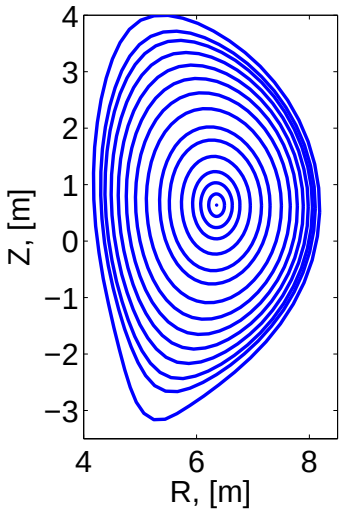

Figure 1: Nested flux surfaces for a 15MA burning plasma in ITER calculated by VMEC.

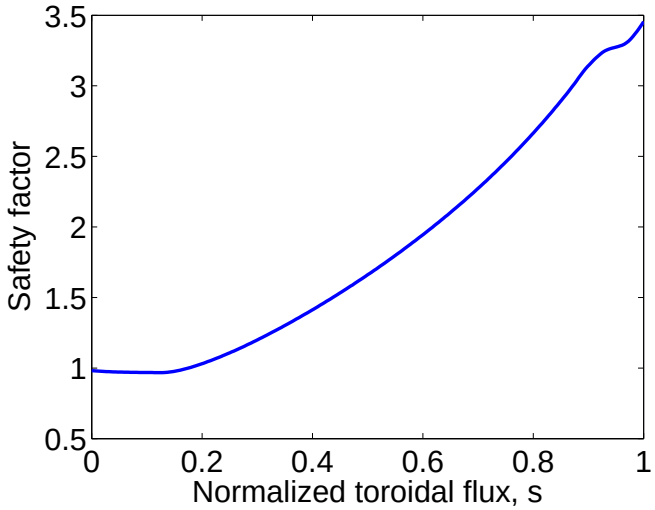

Figure 2: Safety factor for plasma equilibrium in ITER against normalized toroidal flux.

$\phi = 2\pi l/n_{coils}$ where n_{coils} is the number of RMP coils and $l = \{0, 1, 2, ..., n_{coils} - 1\}$ so that

$$I^l_{coil} = I_0 \cos\left(n_{rmp}\left(\frac{2\pi l}{n_{coils}} - \phi_0\right)\right) \tag{3}$$

but we can add another signal at the coil frequency and get the same I^l_{coil} signal

$$I^l_{coil} = I_0 \cos\left((n_{rmp} + kn_{coils})\frac{2\pi l}{n_{coils}} - n_{rmp}\phi_0\right)$$

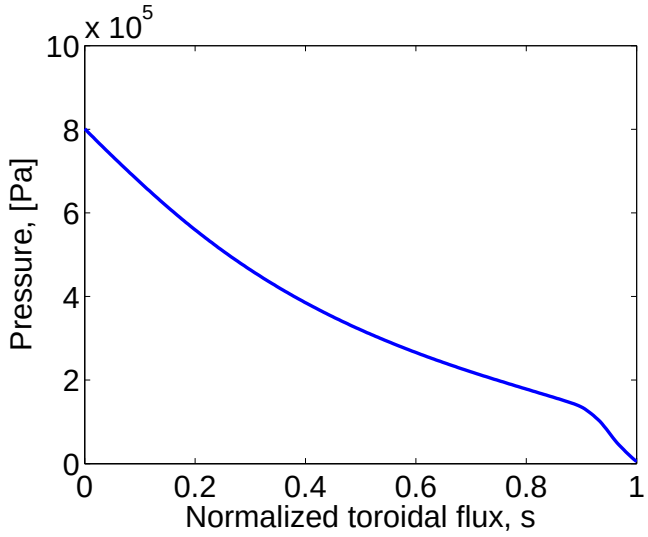

Figure 3: Pressure profile for a 15MA burning plasma in ITER plotted against normalized toroidal flux; high $\vec{\nabla}p$ pedestal at $s \approx 0.95$

$$= I_0 \cos\left(n_{rmp}\frac{2\pi l}{n_{coils}} + 2\pi k l - n_{rmp}\phi_0\right) \tag{4}$$
$$= I_0 \cos\left(n_{rmp}\left(\frac{2\pi l}{n_{coils}} - \phi_0\right)\right)$$

for a given integer k. If we pick $k = -1$ then we have the toroidal harmonic $n_{coils} - n_{rmp}$ being produced. All other harmonics will be greater than n_{coils}.

Further, if we take the signal I^l_{coil} and fourier decompose it we find that we have n_{rmp} and $n_{rmp} - n_{coils}$ harmonics present at equal amplitude. We can use the identity $\cos\alpha + \cos\beta = 2\cos(1/2(\alpha+\beta))\cos(1/2(\alpha-\beta))$ to understand the resulting reconstructed signals. The reconstructed signal is

$$I_{pert} = \frac{1}{2}I_0\cos\left(n_{rmp}(\phi-\phi_0)\right) + \frac{1}{2}I_0\cos\left((n_{rmp}-n_{coils})\phi - n_{rmp}\phi_0\right)$$
$$= \frac{1}{2}I_0\cos\left(n_{rmp}(\phi-\phi_0)\right) + \frac{1}{2}I_0\cos\left((n_{coils}-n_{rmp})\phi + n_{rmp}\phi_0\right) \tag{5}$$
$$= I_0\cos\left(\frac{1}{2}n_{coils}\phi\right)\cos\left(\frac{1}{2}(n_{coils}-2n_{rmp})\phi + n_{rmp}\phi_0\right) \tag{6}$$

Equation (5) shows that if we aim to rotate the applied harmonic by a phase $n_{rmp}\phi_0$ the off harmonic rotates to $-n_{rmp}\phi_0$ i.e. in the opposite direction. Equation (6) shows that the perturbation is no longer a pure harmonic but has an envelop with harmonic $n_{coils} - 2n_{rmp}$. The above results will be used to understand the ITER cases under investigation here.

Figure 4 shows the two fourier harmonics for two different phases of an $n = 4$ applied field, with $n_{coils} = 9$. The left hand plots are for 0^o phase and the right hand plots are for 10^o phase. It can be clearly seen that although the $n = 4$ wave is moving to the right (from the left upper plot to the right upper plot) the perturbation envelop

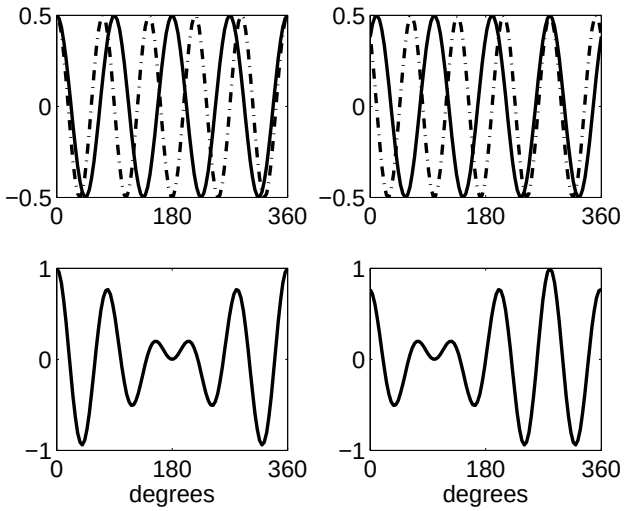

Figure 4: The upper left plot shows the $n = 4$ (solid) and $n = 5$ (dash-dot) harmonics when a zero phase $n = 4$ RMP is applied. The lower left plot shows the sum of these two harmonics. The upper right plot shows the $n = 4$ (solid) and $n = 5$ (dash-dot) harmonics when a 10^o phase $n = 4$ RMP is applied. The lower right plot shows the sum of these two harmonics. Notice that while the $n = 4$ wave moves in one direction the $n = 5$ and the perturbation envelop move in the opposite direction.

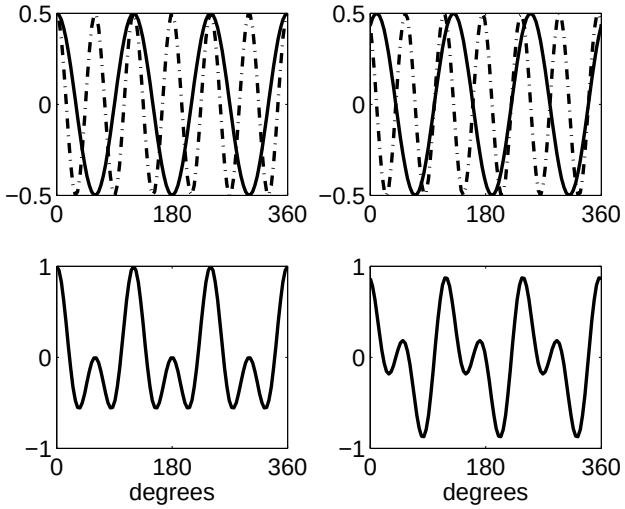

Figure 5: The upper left plot shows the $n = 3$ (solid) and $n = 6$ (dash-dot) harmonics when a zero phase $n = 3$ RMP is applied. The lower left plot shows the sum of these two harmonics. The upper right plot shows the $n = 3$ (solid) and $n = 6$ (dash-dot) harmonics when a 10^o phase $n = 3$ RMP is applied. The lower right plot shows the sum of these two harmonics. Notice that while the $n = 3$ wave moves in one direction the $n = 6$ and the perturbation envelop move in the opposite direction.

has moved to the left (lower plots). Figure 5 shows a similar result for $n = 3$. Notice that while the total $n = 4$ structure rotates rigidly the $n = 3$ structure does not.

We would also expect the strike point splitting pattern on the divertor plate to have the same overall envelop toroidally. This would mean that for the $n = 4$ case the power would be predominantly deposited at one toroidal location which would rotate at a speed determined by the rate of RMP rotation. We would expect the $n = 3$ case to be much less toroidally localized.

2.3. Vacuum field at plasma boundary

In subsection 2.2 an idealized situation was investigated which assumed the current was sampled at point locations toroidally whereas the RMP coils cover a finite region. It also should be noted that the magnetic field of each harmonic produced at the coil may drop off at differing rates. This means that the relative strengths of the harmonics may change from the radial location of the coils to the radial location of the plasma last closed flux surface. We model the plasma with RMP coils in real geometry using VMEC so that we can quantify the relative harmonic drop-offs to see if this effect will be important in ITER. The relative plasma response for the main and sideband harmonics will also be important.

2.4. Static $n_{rmp} = 3$ and $n_{rmp} = 4$

The response of the ITER plasma to $n_{rmp} = 3$ and $n_{rmp} = 4$ RMP configurations are studied first. The configurations studied correspond to the cases designed using the maximum island overlap criterion [5] and also to 'even parity' where the coils at each toroidal location have the same current. These are just examples for illustrative purposes only. Coutour maps showing how the outer boundary has been displaced are shown on the left of: figure 6 for the designed $n_{rmp} = 3$ case, figure 7 for the even parity $n_{rmp} = 3$ case and figure 8 for the designed $n_{rmp} = 4$ case.

We used up to toroidal harmonic $n = 6$ in VMEC for these calculations because, guided by subsection 2.2, there are only nine coils toroidally in each row and so there will be a strong $n_{coils} - n_{rmp}$ harmonic. Thus an applied $n = 4$ will include $n = 5$, and the applied $n = 3$ will include $n = 6$. We also used up to poloidal harmonic $m = 22$, because the plasma response is due in part to the saturation of edge peeling modes. These modes have the same helicity as the field lines hence the maximum poloidal harmonic $\sim nq_a \sim 22$.

The right plot of figure 6 shows the fourier decomposition of the toroidal mode number of the plasma response. This shows that there is a strong $n = 3$ toroidal harmonic as well as a smaller $n = 6$ harmonic. However, this is not always the case for an $n = 3$ applied field. The right plot of figure 7 has a smaller amplitude of $n = 3$ but has a larger absolute and relative $n = 6$ component. The right plot of figure 8 shows a strong $n = 5$ along with the $n = 4$ that is designed.

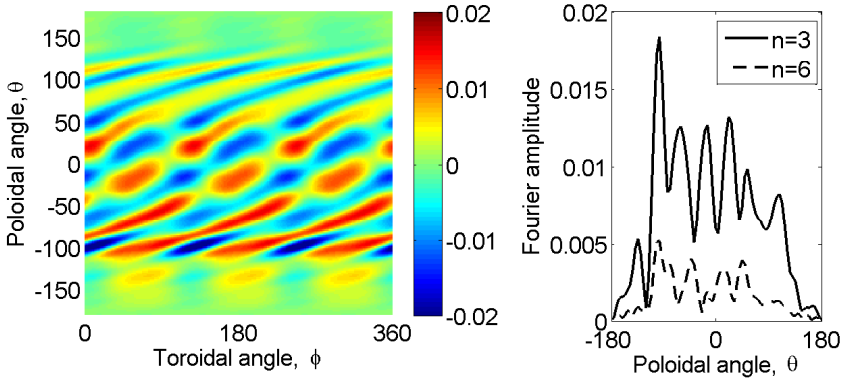

Figure 6: Displacement (m) of outer boundary with the $n_{rmp} = 3$ 'designed' RMP configuration applied (left) and the toroidal fourier decomposition against poloidal angle (right), $n_{coils} = 9$.

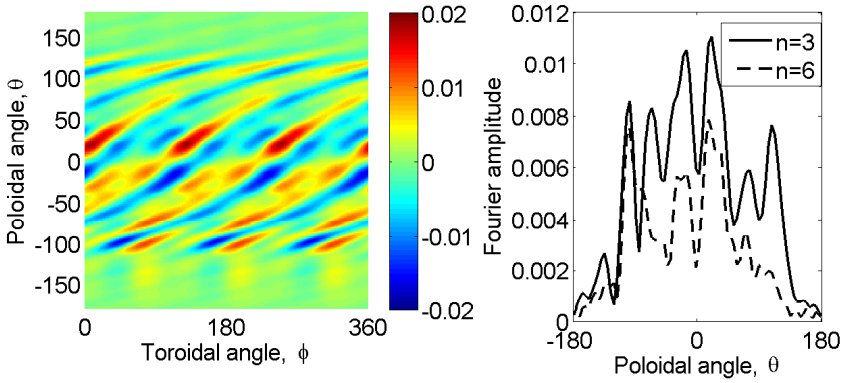

Figure 7: Displacement (m) of outer boundary with the $n_{rmp} = 3$ even parity RMP configuration applied (left) and the toroidal fourier decomposition against poloidal angle (right), $n_{coils} = 9$.

The vacuum field applied to the plasma has a similar amplitude of n_{rmp} and $n_{coils} - n_{rmp}$, however the plasma response to these different harmonics determines the relative strength of the harmonics in the final equilibrium. Certain harmonics may be amplified or damped depending on the plasma and coil configuration.

2.5. Rotating $n_{rmp} = 3$ and $n_{rmp} = 4$ RMPs

It is well known that when RMPs are applied the strike point on the divertor plates splits into a spiral pattern which is locked to the the applied RMP field. ITER will have long pulse operation which may cause very high heat loads over this spiral pattern and so it is proposed that the RMP perturbation will be slowly rotated to ensure even wear of the divertor. This rotation must not come at the cost of reduced ELM control. MAST has demonstrated that ELM control can be achieved while rotating the RMPs [31]. However,

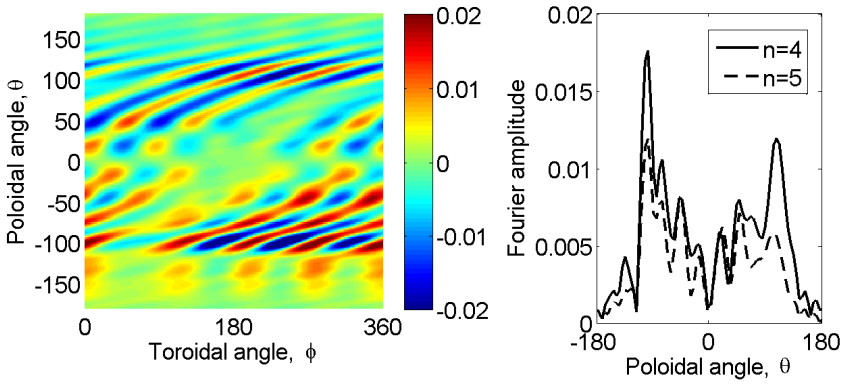

Figure 8: Displacement (m) of outer boundary with the $n_{rmp} = 4$ 'designed' RMP configuration applied (left) and the toroidal fourier decomposition against poloidal angle (right), $n_{coils} = 9$.

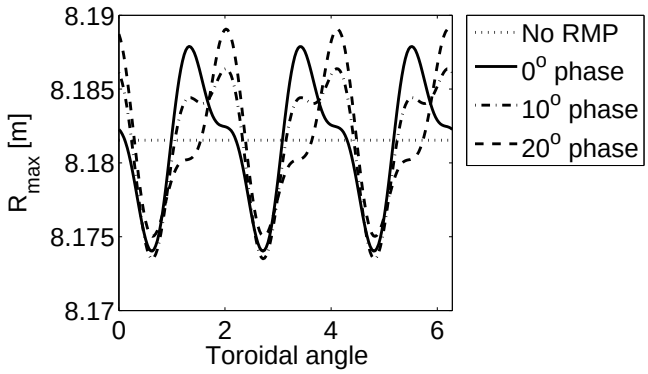

Figure 9: Toroidal variation of the outboard midplane of the plasma as calculated by VMEC with $n_{rmp} = 3$ RMP applied. The absolute phase of the applied RMP is increased in 10^o steps. The shape of the plasma response changes as the RMP rotates.

these experiments were done with 12 coils applying an $n = 3$ perturbation. ITER has fewer coils toroidally and thus, as demonstrated in the previous section, not such a pure applied field and the $n_{coils} - n_{rmp}$ harmonic will rotate in the opposite direction to the n_{rmp} harmonic.

It should be noted that the rotation rate for the RMP will be of the order of a few Hz, whereas the plasma will achieve equilibrium on a much faster timescale than this. This allows us to consider the RMP rotation as a series static equilibria.

Figure 9 shows the radius of the plasma at the outboard midplane as the $n_{rmp} = 3$ is rotated, calculated by VMEC. The changing interference pattern between the $n = 3$ and $n = 6$ harmonics is clear. This is an important effect when modelling the rotation of the RMP. The process of sampling the applied current by the nine RMP coils breaks the symmetry of the problem. This can also be seen in figure 5.

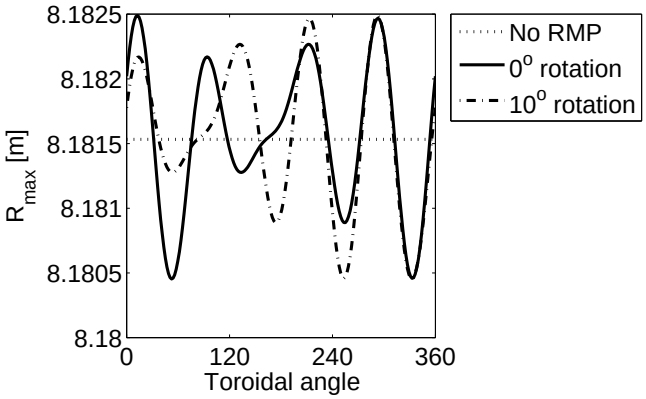

Figure 10: Toroidal variation of the outboard midplane of the plasma as calculated by VMEC with $n_{rmp} = 4$ applied. The rotation of the applied RMP is increased in 10^o steps. The shape of the plasma response does not change with rotation i.e. we have rigid rotation of the perturbation.

Figure 10 shows the radius of the plasma outboard midplane as the phase of the $n_{rmp} = 4$ RMP is changed, calculated by VMEC. Here the shape of the plasma response does not change as the RMP is rotated, however the whole perturbation structure rotates rigidly in the opposite direction to the $n = 4$ harmonic.

We would expect the strike point splitting pattern on the divertor plate also to have an envelop similar to the ones in Figures 9 and 10. This may have important consequences for the heat deposition profile in ITER.

3. Infinite n stability

We study the ballooning stability of the VMEC calculated equilibria here. We use the COBRA [24, 25] code to determine the infinite n ballooning stability especially in the edge region of the plasma where both the pedestal is located and the ELM is thought to be triggered. We also estimate the change in stability in terms of the pressure change required to reproduce the original edge ballooning growth rate profile with no RMP applied. This is a more physical indication of the change in stability. This is done by converting the equilibrium to a fixed boundary and then scaling the whole pressure profile by a given factor. The more the pressure profile has to be reduced to the match the original growth rate the more unstable the RMPs have made the plasma.

3.1. Stability with static $n_{rmp} = 3$ and $n_{rmp} = 4$

We have investigated the infinite n ballooning stability of the $n_{rmp} = 3$ designed case here. Figure 11 shows the ballooning mode growth rate with and without RMPs applied. It can clearly be seen that the application of RMPs destabilizes the infinite n ballooning mode. This is in agreement with results found on both MAST and JET plasmas [4, 26].

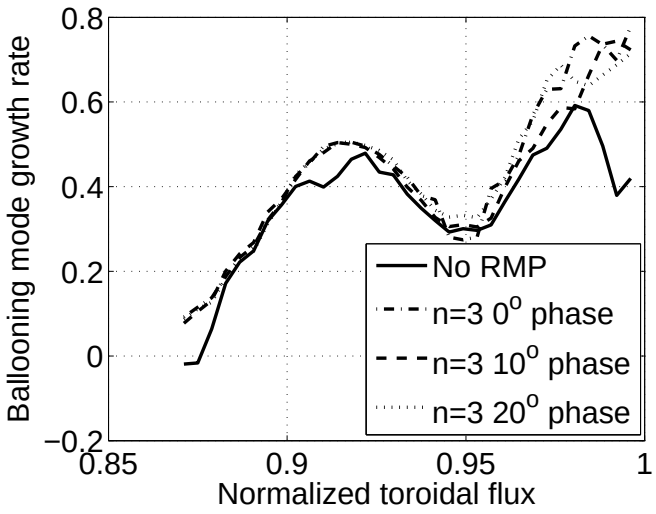

Figure 11: Maximum infinite n ballooning mode growth rate (normalized to Alfven time) against toroidal flux. Solid line is for no RMP applied and dashed, dash-dot and dotted lines show different phases of the $n_{rmp} = 3$ designed case.

We have also calculated the infinite n ballooning stability of the $n_{rmp} = 4$ 'designed' case here. Figure 12 shows the ballooning mode growth rate with and without RMPs applied. It can clearly be seen that the application of RMPs also destabilizes the infinite n ballooning mode.

We have also compared the pressure profile scalings required for both of these cases to reproduce the 'No RMP' growth rate. The scaling factor changes across the profile. In the region $s = 0.87$ to 0.92, where s is the toroidal flux, the $n = 4$ case needs to be scaled by between 95% and 75% while the $n = 3$ needs to be scaled by between 100% (i.e. no change) to 85% indicating that the $n = 4$ configuration is more unstable. In the region $s \geq 0.92$ the pressure scalings reduce from approximately 95% to 85% for both $n = 3$ and $n = 4$. The $n = 3$ case has slightly more fluctuations however.

3.2. Stability with rotating RMPs

We next investigate the effect on plasma stability of rotating the RMP coils. Figure 11 shows the difference in ballooning mode growth rates when there is a 10^o and 20^o rotation for the $n_{rmp} = 3$ case. It can be seen that there is a difference in the ballooning mode growth rates as the RMP is rotated. The region of the difference also changes between these two cases. This is due to the different plasma responses when the RMP is rotated in the $n_{rmp} = 3$ case. We have again compared the pressure profile scalings required for both of these cases to reproduce the 'No RMP' growth rate. In the region $s = 0.87$ to 0.92, all three rotations have similar pressure scalings, scaling by between 100% (i.e. no change) to 85%. In the region $s \geq 0.92$: the 10^o case is the most stable, scaling approximately 100% to 95%; the 0^o is next most stable, scaling approximately

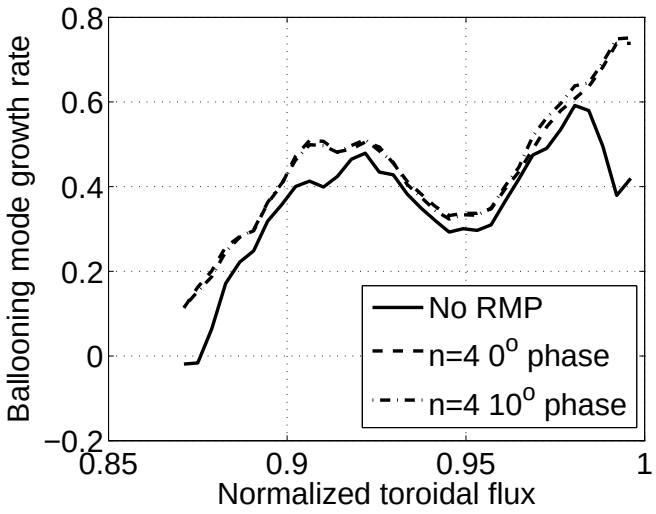

Figure 12: Maximum infinite n ballooning mode growth rate (normalized to Alfven time) against toroidal flux. Solid line is for no RMP applied and the dashed and dash-dot lines show different phases of the $n_{rmp} = 4$ 'designed' case.

90%; and 20^o is least stable, scaling approximately 85% (with some fluctuations around these values).

We next investigate the effect on plasma stability of rotating the $n_{rmp} = 4$ case. Figure 12 shows the difference in ballooning mode growth rates when there is a 10^o rotation for the $n_{rmp} = 4$ case. It can be seen that there is little difference in the ballooning mode growth rates as the RMP is rotated. This is because the perturbation rotates rigidly for the $n_{rmp} = 4$ case.

4. Discussion and Conclusions

4.1. Equilibrium

We have demonstrated in this paper that with only nine coils in the toroidal direction it can be difficult to produce pure toroidal harmonics in the vacuum field of RMPs. The two dominant harmonics n_{rmp} and $n_{coil} - n_{rmp}$ have similar amplitude in the vacuum field. Thus $n_{rmp} = 3$ RMP vacuum field has a significant $n = 6$ harmonic sideband and the $n_{rmp} = 4$ case has a significant $n = 5$ harmonic sideband. However, the $n_{rmp} = 3$ case still produces a vacuum field that is broadly $n = 3$ in character. The $n_{rmp} = 4$ response interferes with the $n = 5$ to produce an $n = 1$ envelop.

It is well known that the plasma responds to the non-axisymmetric vacuum field that is applied to it. In some cases the vacuum field can be amplified and in other cases it can be screened. We have seen above that although the two harmonics are applied with similar amplitude the plasma response does not show both harmonics at the same amplitude. In the $n_{rmp} = 3$ designed case the $n = 6$ harmonic was around 25% of the

$n = 6$ harmonic. This was not true for the even parity $n_{rmp} = 3$ case where the $n = 6$ harmonic was mostly greater than half the $n = 3$ amplitude. In the $n_{rmp} = 4$ designed case the amplitudes of the $n = 4$ and $n = 5$ harmonics in the plasma response were broadly similar. This holds the prospect that we may design the coil configuration such that we can get the desired mix of applied harmonics.

It is well known that RMPs cause strike point splitting, which is locked to the RMP field. This would cause certain toroidal locations to suffer more power deposition than others. This will be mitigated by rotating the RMP field. If the phase of the $n_{rmp} = 3$ field is rotated positively, however, this will simultaneously cause the $n = 6$ perturbation to rotate in the opposite diection. The two perturbations pass through each other causing different plasma responses as the RMP rotates. The $n_{rmp} = 4$ has a large $n = 5$ harmonic, which again moves in the opposite direction. However, the resulting field moves rigidly.

The above work suggests that once criteria for ELM mitigation or suppression have been settled upon we should be able to design a coil configuration that will meet the requirements. However, this will require careful modelling and consideration of all the harmonics that the coils could produce.

We have used VMEC to calculate the plasma response to the RMPs in this paper. We have noted that this model has limitations, for example nested flux surfaces are assumed and there is no plasma rotation etc. However, we believe it still represents a reasonable approximation to the plasma response. We emphasize that the effects seen here should also be seen if other models of plasma response are used even if the absolute response is different.

4.2. Stability

The application of the RMP field causes the infinte n ballooning mode to become more unstable in the plasma edge region. This may either indicate that the peeling-ballooning modes have become more unstable and so ELMs will be more frequent or it may indicate that kinetic ballooning modes will be more unstable. These are known to drive the transport in the pedestal and so limit the pressure gradient.

The ballooning mode growth rate changes as the RMP is rotated for the $n_{rmp} = 3$ case. This indicates that the frequency of ELMs and/or the edge pressure gradient may change as the RMP is rotated. The amount by which the ELM frequency might change by is unknown. This requires further investigation to ensure that the rotation of RMPs in ITER is both safe for the machine and mitigates ELMs as required. Pressure scaling to produce a similar growth rate profile shows that RMP rotation can significantly change the plasma stability, especially in the outer region of the plasma. The $n_{rmp} = 4$ RMP has a constant ballooning mode growth rate with rotation because the plasma response rotates rigidly.

The use of infinite n ballooning mode growth rates to understand finite n stability has limitations. However, the conclusion that ELM mitigation may be altered with

rotation in the $n_{rmp} = 3$ case but not in the $n_{rmp} = 4$ case should be valid for finite n stability analysis.

4.3. Conclusions

The limited number of RMP coils in the toroidal direction on ITER means that any applied RMP field will have a significant 9-n_{rmp} harmonic sideband. It also means that when the RMP is rotated the toroidal shape of the applied RMP field may not be constant, as happens for the $n_{rmp} = 3$. It further means that the infinite n ballooning mode growth rate profile may not be constant with RMP rotation. This may result in the ELM frequency not being consistantly mitigated. However, the RMP field rotates rigidly for the $n_{rmp} = 4$ case so ELM mitigation with RMP rotation should be constant. Unfortunately, the $n_{rmp} = 4$ has a strong $n = 1$ envelop which may cause heat loads to be deposited strongly in one toroidal location. Other effects such as mode locking may also occur. It will be important to understand this topic in more detail so that the ITER first wall is protected.

This paper shows that ensuring that rotating the RMPs both consistantly mitigates the RMPs whilst also spreading the heat load is not straightforward. Further investigation of topics such as finite n peeling ballooning stability, fast particle confinement and robust heat deposition profile on the divertor plate need to be carried out taking into account the effects highlighted in this paper.

Acknowledgements

The authors thank S Hirshman for the use of VMEC and R Sanchez for the use of COBRA. CJH thanks YQ Liu for his comments on the manuscript. RGJC thanks D Ryan & J Simpson for useful discussions. This work has been carried out within the framework of the EUROfusion Consortium and has received funding from the Euratom research and training programme 2014-2018 under grant agreement No 633053. The views and opinions expressed herein do not necessarily reflect those of the European Commission. This project has also received funding from the RCUK Energy Programme [grant number EP/I501045]. To obtain further information on the data and models underlying this paper please contact PublicationsManager@ccfe.ac.uk.

References

[1] Loarte A *et al* 2003 *Plasma Phys. Control. Fusion*, **45** 1549-69
[2] Loarte A *et al* 2014 *Nucl. Fusion*, **54** 033007
[3] Lang P T *et al* 2015 *Plasma Phys. Control. Fusion*, **57** 045011
[4] Chapman IT *et al* 2015 *Plasma Phys. Control. Fusion*, 'ELM control in JET' *accepted*
[5] Evans T E *et al* 2008 *Nucl. Fusion*, **48** 024002
[6] Kirk A *et al* 2013 *Nucl. Fusion*, **53** 043007
[7] Kirk A *et al* 2015 *Nucl. Fusion*, **55** 043011
[8] Connor JW *et al* 1998 *Plasma Phys. Control. Fusion*, **40** 191-213

[9] Wilson H 2002 *Phys. Plasmas*, **9** 1277
[10] Saarelma S *et al* 2011 *Plasma Phys. Control. Fusion*, **53** 085009
[11] Chapman IT *et al* 2012 *Plasma Phys. Control. Fusion*, **54** 105013
[12] Chapman IT *et al* 2014 *Nucl. Fusion*, **54** 083006
[13] Chapman IT *et al* 2014 *Nucl. Fusion*, **54** 123003
[14] Chapman IT *et al* 2014 *Plasma Phys. Control. Fusion*, **56** 075004
[15] Turnbull A 2013 *Phys. Plasmas*, **20** 056114
[16] King J D 2013 *Phys. Plasmas*, **22** 072501
[17] Hirshman SP and Whitson JC 1983 *Phys. Fluids*, **26** 3553-68
[18] Hirshman SP *et al* 1986 *Comp. Phys. Comm.*, **43** 143-155
[19] Orain F *et al* 2014 *Phys. Plasmas* , **20** 102510
[20] Waelbroeck FL *et al* 2012 *Nucl. Fusion*, **52** 074004
[21] Ham CJ *et al* 2015 *Plasma Phys. Control. Fusion*, **57** 054006
[22] Loizu J *et al* 2015 *Phys. Plasmas* , **22** 090704
[23] Lazerson S *et al* 2016 *Phys. Plasmas* , **23** 012507
[24] Sanchez R, Hirshman SP, Whitson JC and Ware AS 2000 *Comput. Phys*, **161** 576-88
[25] Sanchez R, Hirshman SP and Wong HV 2001 *Comput. Phys. Commun*, **135** 82-92
[26] Ham CJ, Chapman IT, Kirk A and Saarelma S 2014 *Phys Plasmas*, **21** 2501
[27] Lazerson SA 2014 *Plasma Phys. Control. Fusion*, **56** 095006
[28] Liu Yueqiang *et al* 2011 *Nucl. Fusion*, **51** 083002
[29] Liu Yueqiang *et al* 2015 *Nucl. Fusion*, **55** 063027
[30] Evans TE *et al* 2013 *Nucl. Fusion*, **53** 093029
[31] Thornton AJ *et al* 2015 *J. Nucl. Mater.*, **463** 723-726